Available online at www.sciencedirect.com
ScienceDirect
Computers and Chemical Engineering 31 (2006) 32–40
Computers & Chemical Engineering
www.elsevier.com/locate/compchemeng

Heat transfer in lid driven channels with power law fluids in a hydrodynamic fully developed flow field

K.-H. Sun [a], D.L. Pyle [b], A.D. Fitt [c,*], C.P. Please [c]

[a] *International Automotive Research Centre, University of Warwick, Coventry, West Midlands CV4 7AL, UK*
[b] *School of Food Biosciences, University of Reading, Reading RG6 6AP, UK*
[c] *School of Mathematics, University of Southampton, Southampton SO17 1BJ, UK*

Received 11 December 2005; received in revised form 7 May 2006; accepted 8 May 2006
Available online 17 July 2006

Abstract

We present a finite element numerical study of heat transfer in lid driven channels with fully developed axial flow for non-Newtonian power law fluids. The effect of channel aspect ratio and material properties on temperature distribution and wall heat transfer are studied. The results show that in comparison with Newtonian fluids the shear thinning property of the fluids acts to reduce the local viscous dissipative heating and as a result the axial local fluid temperature is reduced. Applications of the results to scraped-surface heat exchanger design and operation are recommended.

Keywords: Finite element method; Power law fluid; Viscous dissipation; Lid driven cavity; Scraped-surface heat exchanger

1. Introduction

This study concerns flow and heat transfer in lid driven channels. As well as a purely theoretical importance (Shankar & Deshpande, 2000), such flows are directly relevant to many complex industrial applications, such as screw extruders (Kokini, Ho, & Karwe, 1992) and scraped-surface heat exchangers (SSHEs) (Harrod, 1986). Though there are major differences between all of these industrial processes, they may be classified together in the sense that the flows involved can almost invariably be characterised as low Reynolds number/high Prandtl number flows of highly viscous non-Newtonian fluids. Many previous studies have concerned such flows. Numerous 2D studies examined the flow of Newtonian fluids in lid driven cavities (see, for example, Burggraf, 1966; Nallasamy & Prasad, 1977; Pan & Acrivos, 1967). A range of non-Newtonian materials, such as viscoelastic fluids (Grillet, Yang, Khomani, & Shaqfeh, 1999), Bingham fluids (Mitsoulis & Zisis, 2001) and power law fluids (Martin, 1969) have also been analysed in a two-dimensional setting. Though such studies can contribute much understanding, for non-Newtonian fluids the tangential and the axial flows in such devices are coupled. It is therefore important to know the consequences of axial flow and, in particular, how the tangential (cross) flow interacts with the axial flow. Asymptotic results for a three-dimensional isothermal flow in an SSHE were derived by Fitt & Please (2001) and Karwe & Jaluria (1990) carried out numerical studies of heat transfer within a single screw extruder. In both Fitt & Please (2001) and Karwe & Jaluria (1990), simplifications were made by assuming creeping flow of power law fluids with small annular-gap/perimeter ratios so that the sidewall effects could be neglected.

The role of viscous dissipation in steady-state 2D forced convection heat transfer was investigated numerically for lid driven cavities (Sun et al., submitted for publication). A further study (Sun et al., 2004) extended the work of Sun et al., submitted for publication to include the effects of shear thinning and realistic SSHE geometry. A key conclusion from Sun et al., submitted for publication was that, at the singularity corners of the flow region, the apparent viscosity, fluid temperature and viscous dissipation were all smaller for shear thinning fluids compared to the Newtonian case. Quasi-three-dimensional effects (i.e. assuming an axial hydrodynamic fully developed flow) were included in a numerical study of an isothermal lid driven channel in Sun et al. (2006). The results reported in Sun et al. (2006) showed that for hydrodynamic fully developed flow, both the pressure drop and flow field were dependent on the channel aspect ratio, power law index, the tangential and axial Reynolds numbers and their ratios. Similar to previously reported results in ducts (see, for

* Corresponding author. Tel.: +44 23 8059 5141; fax: +44 23 8059 5147.
E-mail address: adf@maths.soton.ac.uk (A.D. Fitt).

0098-1354/$ – see front matter © 2006 Elsevier Ltd. All rights reserved.
doi:10.1016/j.compchemeng.2006.05.005

Nomenclature

A	channel aspect ratio H/L
Br	Brinkman number $Br = \mu_F U^2/k\Delta T$
c_1 and c_2	constants in viscosity model (5)
C_p	specific heat at constant pressure (J/(kg K))
d_{ij}	infinitesimal rate-of-strain tensor $1/2(\partial u_i/\partial x_j + \partial u_j/\partial x_i)$
D_h	hydraulic diameter $2HL/(H+L)$ (m)
f	friction factor
H	channel height (m)
I_2	second invariant of the rate of deformation tensor $2d_{ij}d_{ij}$ (s^{-2})
k	thermal conductivity (W/m K)
L	lid side channel length (m)
m	consistency index (Pa s^n)
n	shear thinning or power law index
Nu	local axial averaged heat flux on the lid $Nu = \int_0^1 q^* \, dx^*$
Nu_m	modified local axial averaged heat flux on the lid $Nu_m = (T_{in} - T_w)/(T_m - T_w)Nu$
p	pressure (N/m^2)
$-p_z$	axial pressure gradient (N/m^3)
Pe_U	U-Peclet number $Pe_U = Re_U Pr = \rho U L C_p/k$
Pe_W	W-Peclet number $Pe_W = Re_W Pr = \rho W L C_p/k$
Pr	Prandtl number $Pr = C_p\mu_F/k$
q	heat flux (W/m^2)
q^*	non-dimensional local axial lid heat flux $q^* = qL/k\Delta T = -\partial T^*/\partial y^*|_{y^*=A}$
Re_U	Reynolds number $Re_U = \rho UL/\mu_F$
Re_W	Reynolds number $Re_W = \rho WL/\mu_F$
S	channel cross-sectional area (m^2)
T	temperature (°C)
T_{in}	inlet temperature (°C)
T_m	fluid bulk–mean temperature (°C)
T_w	lid temperature (°C)
ΔT	temperature difference magnitude $\lvert T_{in} - T_w \rvert$ (°C)
u	x-component of velocity (m/s)
U	lid velocity (m/s)
v	y-component of velocity (m/s)
w	z-component of velocity (m/s)
W	average axial velocity (m/s)
x, y, z	cartesian coordinates (m)
Z	non-dimensional thermal axial distance $Z = z/(D_h Pe_w)$

Greek symbols

α	velocity ratio or Reynolds number ratio W/U
Γ	shear rate (s^{-1})
μ	absolute dynamic viscosity (Pa s)
μ_F	characteristic dynamic viscosity (Pa s)
ρ	density (kg/m^3)

Superscript

*	non-dimensional value

example, Hartnett & Kostic, 1989), though this study concerned turbulent rather than laminar flow), the results of Sun et al. (2006) also confirmed that for (laminar) flow in a lid driven channel a notable "drag reduction effect" (resulting in a reduced axial pressure gradient) was found with shear thinning power law fluids. However, at high tangential Reynolds numbers it was also found that the tangential flow causes strong distortion in the axial flow so that the drag reduction effect was reduced or even reversed.

The current study further generalises the work discussed above by considering quasi-3D heat transfer for power law fluids in lid driven channels with hydrodynamic fully developed laminar flow. The general *modus operandi* is as follows: under the assumption of a temperature independent viscosity, the fully developed velocity field may be determined first (decoupled with temperature) as in Sun et al. (2006). Neglecting the axial conduction term in the energy equation, the temperature field is then calculated using a marching scheme.

Consistency checks are carried out by comparing the numerical results with available published results. The computations cover a range of physical and non-dimensional parameters, including power law index, channel aspect ratio, tangential velocity, Brinkman number, axial Peclet number and thermal boundary (heating/cooling) conditions. In each case, the temperature distributions, axial local average temperature and axial local heat flux are given. The main aim of the work is to understand the characteristics of heat transfer in a lid driven device such as an SSHE when the effects of wall heating, (quasi-3D), fully developed axial flow and the presence of shear-thinning fluids must all be taken into account.

2. Differential equations and numerical procedure

2.1. Governing equations

Typical fluids processed in SSHEs and extruders are characterised by relatively large viscosities and high Prandtl numbers. An important consequence of this is that the thermal boundary layer is much thinner than the velocity boundary layer. For this reason, the assumption that the velocity profile is fully developed before the fluid enters the heating zone is justified. For materials with temperature independent viscosity, this further implies that the velocity field does not change with either axial location or thermal boundary conditions.

2.1.1. Flow equations and boundary conditions

A rectangular coordinate system is used with origin at the upstream bottom left hand corner of the channel (see Fig. 1 for details). The x–y plane is normal to the axial flow direction and the z-axis is in the direction of the axial flow. The velocity components are denoted by u, v and w, respectively. The channel lid, of width L, is located at the top of the channel ($y = H$) and moves with speed U in the positive x direction. The channel aspect ratio is denoted by $A = H/L$. Representative velocity scales are the lid velocity U (for the tangential velocity components u and v), and the average axial velocity W (for the axial velocity component w). The scales for length and pressure are the lid length L and $\mu_F U/L$, respectively. We also assume that a characteristic

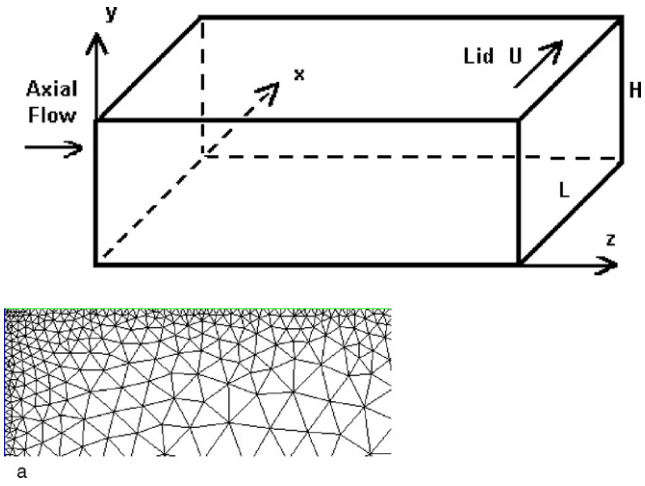

Fig. 1. (a) Schematic view and coordinate system and (b) magnified view of corner mesh concentration near sidewall/lid corner.

viscosity μ_F is the viscosity at a given shear rate:

$$\Gamma = \left(\left(\frac{U}{L} \right)^2 + \left(\frac{W}{L} \right)^2 \right)^{1/2}.$$

Throughout this study, we assume that the characteristic viscosity μ_F is independent of temperature so that the momentum and the energy equations can be decoupled. (Although many of the materials processed in SSHEs in reality have strongly temperature-dependent viscosities, in the current study we wish to concentrate particularly on shear-thinning effects.) Assuming a laminar, steady flow of an incompressible viscous fluid with fully developed axial flow in an infinitely long channel, it is reasonable to assume that all the velocity components are functions of x and y only. The z-momentum equation then shows that the axial pressure gradient is also independent of z. At any cross-section in the x–y plane, the governing equations for the velocity and pressure are therefore:

$$\frac{\partial u^*}{\partial x^*} + \frac{\partial v^*}{\partial y^*} = 0, \tag{1}$$

$$Re_U \left(u^* \frac{\partial u^*}{\partial x^*} + v^* \frac{\partial u^*}{\partial y^*} \right) = -\frac{\partial p^*}{\partial x^*} + \frac{\partial}{\partial x^*} \left(\frac{\mu}{\mu_F} \frac{\partial u^*}{\partial x^*} \right) + \frac{\partial}{\partial y^*} \left(\frac{\mu}{\mu_F} \frac{\partial u^*}{\partial y^*} \right), \tag{2}$$

$$Re_U \left(u^* \frac{\partial v^*}{\partial x^*} + v^* \frac{\partial v^*}{\partial y^*} \right) = -\frac{\partial p^*}{\partial y^*} + \frac{\partial}{\partial x^*} \left(\frac{\mu}{\mu_F} \frac{\partial v^*}{\partial x^*} \right) + \frac{\partial}{\partial y^*} \left(\frac{\mu}{\mu_F} \frac{\partial v^*}{\partial y^*} \right), \tag{3}$$

$$Re_U \left(u^* \frac{\partial w^*}{\partial x^*} + v^* \frac{\partial w^*}{\partial y^*} \right) = f Re_W + \frac{\partial}{\partial x^*} \left(\frac{\mu}{\mu_F} \frac{\partial w^*}{\partial x^*} \right) + \frac{\partial}{\partial y^*} \left(\frac{\mu}{\mu_F} \frac{\partial w^*}{\partial y^*} \right). \tag{4}$$

Here, asterisk indicates that the variables are in their non-dimensional form, $Re_U = \rho UL/\mu_F$ is the tangential flow Reynolds number and $Re_W = \rho WL/\mu_F$ is the axial flow Reynolds number (which may also be thought of as a non-dimensional axial volume flux). The non-dimensional axial pressure gradient or friction factor is denoted by $f = -p_z L/\rho W^2$, and the frictional pressure gradient is defined by:

$$f Re_W = \frac{-p_z L^2}{\mu_F W}.$$

We define the velocity (or Reynolds number) ratio as $\alpha = W/U = Re_W/Re_U$. In most industrial applications, such as SSHEs and screw extruders, the tangential flow is dominant, the axial velocity often being less than 1/5 of the tangential velocity. Velocity ratios of 0.2 were therefore used for the results calculated in Section 3.

The boundary conditions in the plane of the tangential flow are $u^* = 1$, $v^* = w^* = 0$ at the channel lid, and $u^* = v^* = w^* = 0$ at the other channel walls.

For the viscosity, we assume a generalized shear thinning power law: $\mu = m I_2^{(n-1)/2}$. Here, I_2 is the second invariant of the shear rate tensor and m and n are the consistency index (Pa s^n) and shear-thinning index, respectively. A typical value of n for food materials processed in SSHEs such as fruit jam, peanut butter, etc., is 0.33 (see, for example, Fitt & Please, 2001). The value $n = 1.0$ (Newtonian fluid) is also considered for completeness. Non-dimensionalized by the characteristic viscosity

$$\mu_F = m \left(\left(\frac{U}{L} \right)^2 + \left(\frac{W}{L} \right)^2 \right)^{(n-1)/2},$$

the final form of the viscosity is:

$$\frac{\mu}{\mu_F} = \left(\frac{I_2^*}{1+\alpha^2} + c_1 \right)^{(n-1)/2} + c_2 \tag{5}$$

where

$$I_2^* = \left(2 \left(\frac{\partial u^*}{\partial x^*} \right)^2 + 2 \left(\frac{\partial v^*}{\partial y^*} \right)^2 + \left(\frac{\partial u^*}{\partial y^*} + \frac{\partial v^*}{\partial x^*} \right)^2 + \alpha^2 \left(\frac{\partial w^*}{\partial x^*} \right)^2 + \alpha^2 \left(\frac{\partial w^*}{\partial y^*} \right)^2 \right)$$

and

$$I_2 = \frac{U^2}{L^2} I_2^*.$$

The constants c_1 and c_2 are included in Eq. (5) to ensure that the viscosity is non-zero and finite everywhere. Values of $c_1 = 0.000001$ and $c_2 = 0.0001$ were used for all computations; numerical experiments show that this modification has an insignificant effect on the viscosity whilst giving physically reasonable viscosity values.

2.1.2. Energy equation and thermal boundary conditions

We assume that the entering stream has a uniform temperature T_{in}, the lid temperature is maintained at a constant temperature

T_w, the other walls are adiabatic and the axial conduction term can be neglected. The non-dimensional temperature is defined as $T^* = (T - T_w)/\Delta T$, where $\Delta T = |T_{in} - T_w|$. (The absolute value is used so that the value of Brinkman number is positive for both cooling and heating.) The thermal properties of the flow are determined by heating or cooling from the lid, heat carried by the fluid and the heat generated by viscous dissipation. The non-dimensional energy equation is:

$$Pe_U \left(u^* \frac{\partial T^*}{\partial x^*} + v^* \frac{\partial T^*}{\partial y^*} \right) + Pe_W w^* \frac{\partial T^*}{\partial z^*} = \frac{\partial^2 T^*}{\partial x^{*2}} + \frac{\partial^2 T^*}{\partial y^{*2}} + Br \left(\frac{\mu}{\mu_F} \right) I_2^* \quad (6)$$

where Pe_U and Pe_W are the Peclet numbers corresponding to the tangential and axial flows, respectively (see nomenclature table for definitions) and Br is the Brinkman number $Br = \mu_F U^2/k\Delta T$.

The thermal boundary conditions are that the lid $y^* = A$ is isothermal ($T^* = 0$ at $y^* = A$), the other channel walls are adiabatic ($\partial T^*/\partial x^* = 0$ at $x^* = 0$ and 1, $\partial T^*/\partial y^* = 0$ at $y^* = 0$). At $z^* = 0$, the initial condition is that $T = T_{in}$, so that $T^* = 1$ ($T_{in} > T_w$ for cooling) and $T^* = -1$ ($T_{in} < T_w$ for heating).

2.1.3. Local axial heat flux

At a given axial location, the lid heat flux (a localised quantity) and fluid bulk–mean temperature (which involves the whole of the cross-sectional area) provide two related but different measures of the local heat transfer between the lid and the fluid. The local axial lid heat flux at a location z is defined as $q = -k(\partial T/\partial y)|_{y=H}$. The fluid bulk–mean temperature T_m is an axial/longitudinal flow-weighted average of the local fluid temperature defined for a given channel cross-sectional area S by:

$$T_m = \frac{\int_S wT \, dS}{\int_S w \, dS}.$$

In contrast to the dimensionless hydrodynamic axial distance $z^* = z/L$, the dimensionless thermal axial distance is defined as $Z = z/(D_h Pe_w)$ where D_h is the hydraulic diameter $2HL/(H + L)$. Many of the results presented below will be plotted as a function of Z rather than z^*, since this is the natural axial coordinate as far as heat transfer is concerned. The dimensionless local axial heat flux on the lid is $q^* = qL/k\Delta T = -\partial T^*/\partial y^*|_{y^*=A}$; q^* will be positive for cooling and negative for heating conditions. The local axial lid heat flux Nu refers to the averaged value of q^* on the lid and is defined by $Nu = \int_0^1 q^* \, dx^*$.

As described above, in the current computations the effects of temperature on the fluid viscosity have been neglected. The heat produced by viscous dissipation therefore depends only on the velocity field and the Brinkman number, and has the same magnitude for both heating and cooling conditions. Without viscous dissipation ($Br = 0$), the absolute value of local lid heat flux is the same for heating and cooling conditions. Far enough downstream, the bulk fluid temperature will eventually reach the lid temperature. The thermally fully developed value of Nu will therefore be zero and independent of the fluid properties and operation conditions. A modified non-dimensional lid heat flux may be defined by $Nu_m = (T_{in} - T_w)/Nu(T_m - T_w)$. In contrast to Nu, at thermally fully developed conditions, Nu_m is a non-zero constant whose value depends on power law index, Brinkman number etc. Note, however, that if viscous dissipation is present ($Br \neq 0$), then at sufficiently large axial locations the fluid bulk–mean temperature will eventually reach and exceed the lid temperature (The initial heating will change to cooling of the fluid) so that Nu_m will be singular at $T_m = T_w$. In the current study viscous dissipation plays an important role ($Br \neq 0$) so most of the results are presented in terms of Nu (though we also use Nu_m for comparison purposes). Unless otherwise specified, all results presented in this text are given as non-dimensional values with the asterisk is omitted for brevity.

2.2. Numerical formulation and solution procedure

To solve Eqs. (1)–(4) and (6) numerically, we used the commercial finite element partial differential equation solver Fastflo™ (Fastflo, 2000). It should be stressed that this is not a "black box" CFD package. Appropriate numerical methods have to be selected and implemented by the user. The basic methodology used for the velocity computations is the same as that used in previous studies (see Sun et al., 2006 for a detailed discussion). A mesh of 3470 six-noded triangular elements was used, the mesh being concentrated at all boundaries and singularity corners. An illustrative diagram of the mesh concentration at a sidewall/lid interface is shown in Fig. 1b. Once the velocity has been determined, the temperature may be calculated from the energy equation and associated boundary conditions using a marching scheme. At the inlet to the channel a sudden change of temperature will occur owing to the fact that the lid temperature T_w and the inlet temperature T_{in} are in general different. If a simple scheme such as the Crank–Nicolson algorithm is used here it is known that axial heat flux oscillations may occur. To avoid such undesirable effects, we therefore used an implicit Euler scheme (see, for example, Sun et al., submitted for publication). In all computations, the axial increment step was determined through numerical experiments to ensure reliable results.

To check our numerical procedure, computations were first made in a square duct without viscous dissipation (i.e. a square cavity with a stationary lid with $Re_U = 0$ and $Br = 0$). To allow comparisons with published data, the thermal boundary conditions in this case were specified with all the walls heated at a constant temperature T_w. In a duct with hydrodynamic fully developed laminar flow and with temperature independent viscosity, the magnitude of local axial heat flux is the same (i.e. independent of Pe_W) at the same dimensionless thermal axial location Z (Hartnett & Kostic, 1989). The local axial heat flux increases with decreasing shear thinning index n and decreasing duct aspect ratio A. For $n = 1$ and 0.5, a comparison between our computed results and the computational results of Chandrupatla and Sastri (1997) of axial local heat flux Nu_m is shown in Fig. 2. It is seen that very good agreement is obtained between the current computations and the published results (Chandrupatla & Sastri, 1997). In the absence of viscous heating, the wall heat flux is primarily a function of the near wall velocity gradient. Predictably, therefore, the results of Fig. 2 show that the wall

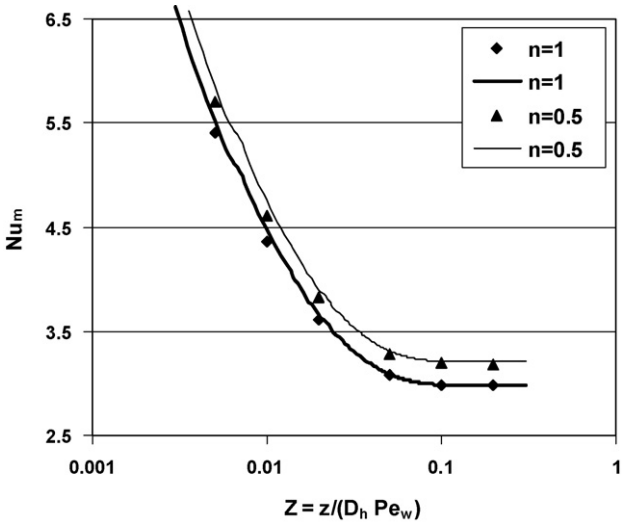

Fig. 2. Modified wall heat flux Nu_m in duct flow. Lines: computed values; symbols: Chandrupatla and Sastri (1997).

heat flux (Nu_m) is therefore higher for more strongly shear thinning fluids (where larger near wall velocity gradients are present) than for Newtonian fluids.

2.3. Numerical convergence

A brief discussion on numerical convergence is apposite: the work reported here is essentially a non-isothermal extension of the work contained in Sun et al. (2006), where many of the key issues regarding both convergence and accuracy are discussed more fully. As in Sun et al. (2006), the sensitivity of the results to the mesh size and convergence criteria were checked in some detail. Richardson extrapolation was applied to the values of the pressure gradient for a group of four selected grids to obtain a final value or higher accuracy than that for even the finest grid. In this way, it was determined that the mesh concentration described above and illustrated in Fig. 1b, along with a mesh of 3470 six-noded triangular elements led to results that provided sufficient resolution at the centre of the channel, while also allowing suitable resolution in the boundary layers for the Reynolds numbers covered in these computations.

As in Sun et al. (2006), numerical experiments showed that the results and the convergence were not very sensitive to the initial distributions of the axial and tangential velocity: the computational time required depends mainly on the channel aspect ratio and the Peclet number.

3. Results and discussion

For power law fluids, the non-dimensional parameters are interdependent. For instance, if the lid velocity is altered then the Reynolds number, Peclet number and Brinkman number will all be different. Parametric studies were therefore carried out in two different ways. One was to change individual non-dimensional quantities. The other was to change individual physical parameters for scale-up purposes.

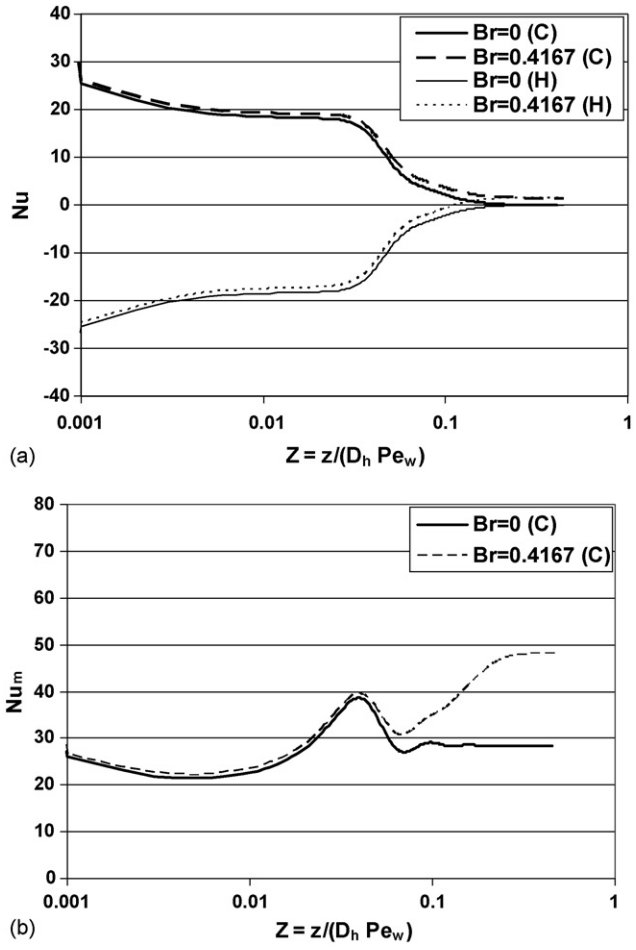

Fig. 3. Effect of Br and thermal boundary conditions on lid heat flux for power law fluids with $n = 0.33$. Heating (H) and Cooling (C): $Re_U = 10$, $Pe_W = 100$, $A = 0.5$ and $W/U = 0.2$: (a) Nu vs. Z and (b) Nu_m vs. Z.

3.1. The effect of viscous dissipation on heat transfer for $n = 0.33$ and 1.0

The effects of viscous dissipation (Brinkman number) and heating/cooling on Nu and Nu_m (for $Re = 10$, $Pe_W = 200$) are shown for power law fluids ($n = 0.33$) as a function of distance along the channel in Fig. 3. Equivalent results for Newtonian fluids ($n = 1.0$) are shown in Fig. 4. (Because of the singularity in Nu_m described in Section 2.1.3 above, only cooling conditions are shown in Figs. 3b and 4b.)

Without viscous heating ($Br = 0$), the absolute value of the wall heat flux Nu should be the same for heating or cooling, a hypothesis confirmed by the results of Figs. 3 and 4. For non-zero viscous dissipation, extra heat needs to be taken out of the lid to cool the fluid material while less heat input is required to heat up the fluid material. Therefore, for a given axial flow and fixed values of n, A, Re and Pr, the local axial lid heat flux Nu should increase with increasing Brinkman number. Figs. 3 and 4 show that this effect is much more pronounced for Newtonian flow (Fig. 4), where the dissipation is larger in the near-corner regions.

We also note that for $Br = 0$, the "fully developed" ($Z \rightarrow 1$) value of Nu_m is smaller for $n = 1.0$ (Fig. 4) than $n = 0.33$ (Fig. 3);

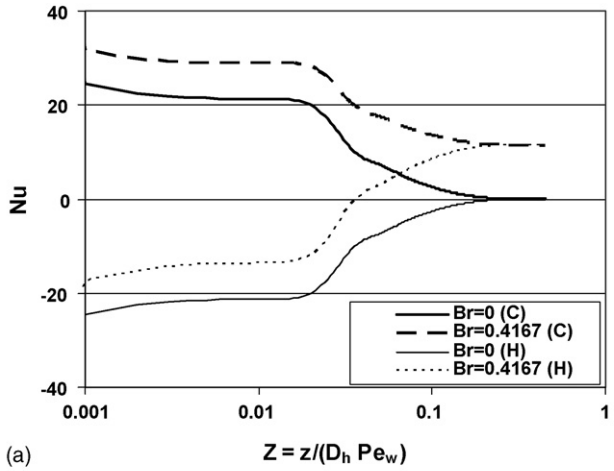

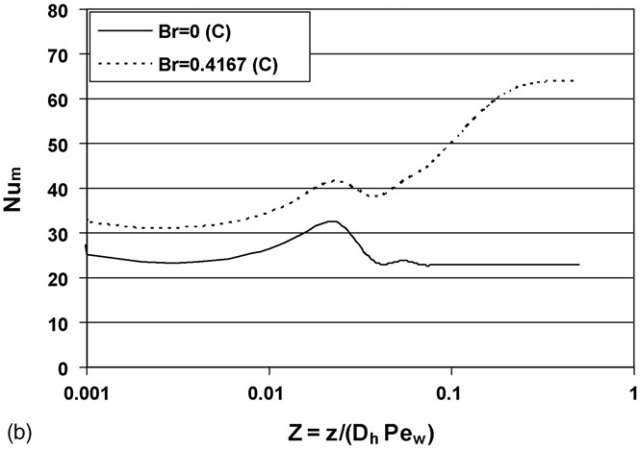

Fig. 4. Effect of Br and thermal boundary conditions on lid heat flux for Newtonian fluids with $n = 1.0$. Heating (H) and cooling (C): $Re_U = 10$, $Pe_W = 100$, $A = 0.5$ and $W/U = 0.2$. (a) Nu vs. Z and (b) Nu_m vs. Z.

this is consistent with the duct flow results in Fig. 2. However, with viscous heating ($Br = 0.4167$), this effect appears to reverse since now Nu_m is larger for Newtonian than non-Newtonian flow. This phenomenon may again be ascribed to the larger heat dissipation in the near-corner regions that may be expected in Newtonian fluids.

Fig. 5 shows the bulk–mean temperature T_m (for the same conditions as Figs. 3 and 4) when viscous heating is present ($Br = 0.4167$). The result that the wall heat flux Nu at a given axial location Z is lower for power-law fluids than for the case $n = 1$ (see Figs. 3 and 4) is repeated in the corresponding bulk–mean temperature in Fig. 5.

Moreover, when comparing the lid heat fluxes for $Br = 0.4167$ and $Br = 0$ in Figs. 3 and 4, a bigger difference is found for $n = 1.0$ than for $n = 0.33$ for the same thermal boundary condition (heating or cooling). This difference is once again a manifestation of the details of shear-thinning flow; in the energy equation, the viscous dissipation term is determined by local velocity gradients and the local effective viscosity. In a lid driven channel, close to the singularity corners the velocity gradients are very high. The viscous dissipation is therefore relatively large for constant viscosity Newtonian fluids. However, for shear thinning fluids the local effective viscosity is reduced in high shear

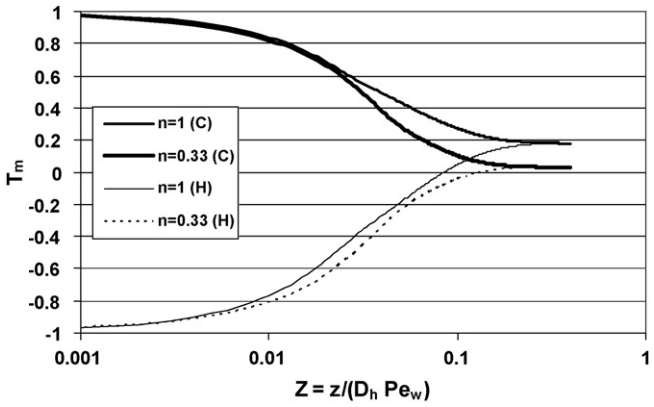

Fig. 5. Effect of n on fluid bulk–mean temperature. Heating (H) and cooling (C): $Re_U = 10$, $Br = 0.4167$, $Pe_W = 100$, $A = 0.5$ and $W/U = 0.2$.

regions, and the combined effects of high shear and low viscosity result in smaller viscous dissipation. This is consistent with the 2D results in (Sun et al., 2004; Sun et al., submitted for publication). This effect is important in the general context of SSHEs and such devices, for it explains the experimental results of Harrod (1986) in SSHEs. These showed that heat transfer is different for heating and cooling conditions with bigger differences found for Newtonian fluids. It is not surprising that these results are also supported by numerical results for creeping flow in a single screw extruder in Karwe and Jaluria (1990).

Finally, Figs. 3 and 4 also show that the values of Nu decrease in magnitude as the thermal boundary layer thickens in the axial direction, and, for heating, the sign of the lid heat flux changes from negative at the thermal entrance region to positive for the thermally fully developed case. The behaviour of the parameter Nu_m is somewhat different, however, for in all the four cases considered we observe a local maximum in Nu_m at about $Z = 0.05$. Our numerical experiments show that the shape of the Nu_m curve varies with the channel aspect ratio and the Peclet number. The peak coincides with the temperature distributions at specific downstream axial locations where, due to tangential circulation, fresh fluid material with a temperature close to the inlet temperature is moved closer to the heat transfer surface at the lid. This coincides with a sharp reduction in both the results for Nu (Figs. 3 and 4), and those for T_m (Fig. 5). The existence and axial location of this peak and the associated sudden drop in Nu is evidently an important matter for those who both design and operate SSHEs and other related devices.

3.2. The effect of specific heat, channel aspect ratio, characteristic viscosity and lid velocity on heat transfer

In Figs. 6–8, results are presented in terms of dimensional quantities to indicate the range of interest for scale-up.

Fig. 6a quantifies the effects of variable Peclet number Pe_W (i.e. change of specific heat C_p) on the lid heat flux Nu for (cooling of) power law fluids with $n = 0.33$ at $Re_U = 10$ and $Br = 0.4167$ ($U = 1.0$ and $W = 0.2$). In the thermal entrance region of a lid driven channel, the local axial lid heat flux is evidently strongly dependent on the Peclet number. For $Pe_W = 2000$, the

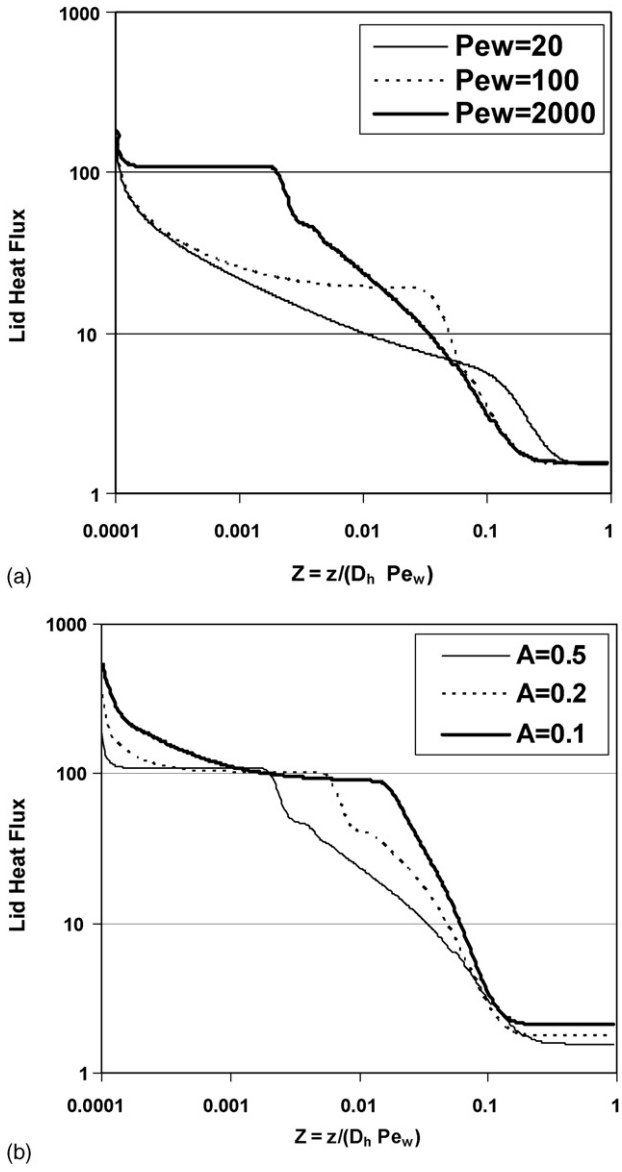

Fig. 6. Lid heat flux *Nu* for cooling of power law fluids with $n = 0.33$, $Re_U = 10$, $Br = 0.4167$ and $W/U = 0.2$: (a) effect of Peclet number Pe_W and (b) effect of cavity aspect ratio A.

heat flux is virtually constant for $Z < 0.005$. It then decreases rapidly before reaching its fully developed value at about $Z = 0.3$. For $Pe_W = 100$, a decrease in lid heat flux is apparent in the thermal entrance region before a plateau is again reached at about $Z = 0.05$; thereafter a rapid decrease in lid heat flux again takes place. For $Pe_W = 20$, the "plateau" effect is much less pronounced and the lid heat flux decreases both more smoothly and rapidly before the thermally fully developed value is attained. The Peclet number measures the relative importance of convection and conduction in the overall heat transfer process. For large Pe_W convection dominates and the flow is composed largely of closed streamlines; the tangential (u,v) flow constantly transfers fresh liquid to the lid region so that high local heat transfer effects can persist. As Pe_W decreases the heat is able to penetrate into the centre of the cavity much faster thereby reducing the local lid heat transfer for small Z. This behaviour is clarified by the

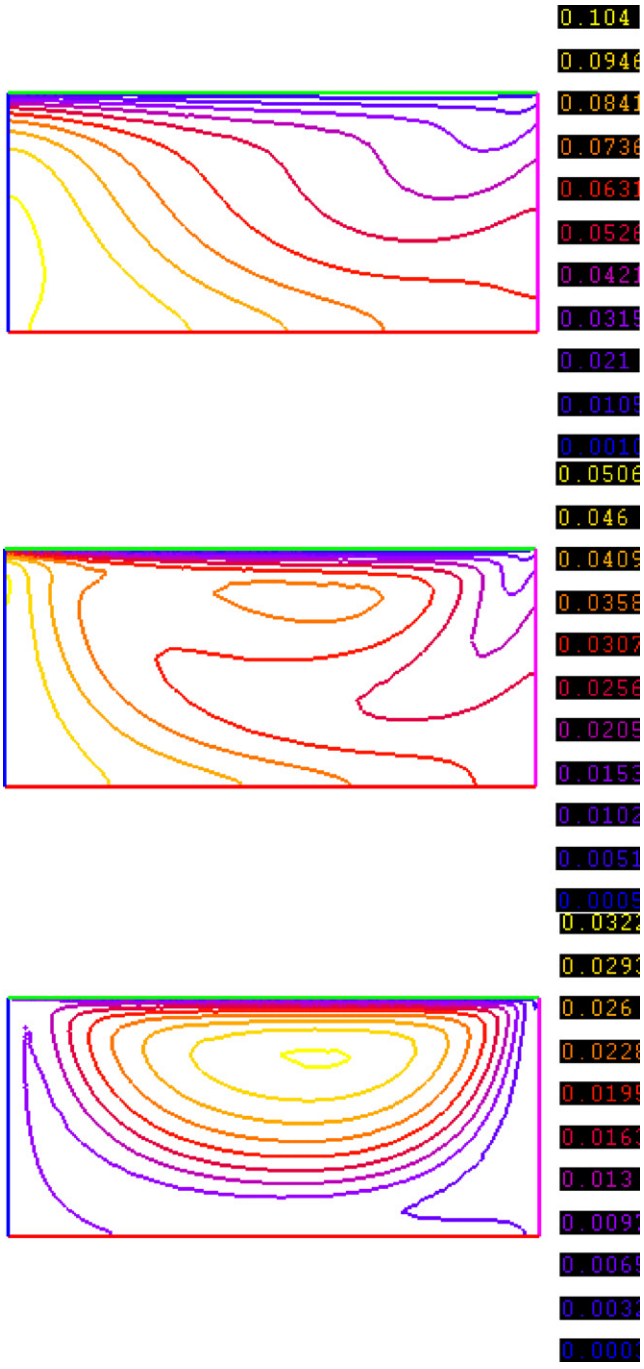

Fig. 7. Fully developed temperature distributions for power law fluids with $n = 0.33$ and $Re_U = 10$, $Br = 0.4167$, $A = 0.5$, $W/U = 0.2$: (top; $Pe_W = 20$), (centre; $Pe_W = 100$) and (bottom; $Pe_W = 2000$).

thermally developed temperature distributions corresponding to Fig. 6a which are shown in Fig. 7. The virtually closed temperature contours for $Pe_W = 2000$ indicate that the heat is trapped and that the tangential flow contains stagnation zones (see Sun et al., 2006). It should be noted that the results of Fig. 6a not only show different heat transfer characteristics for the duct flow considered earlier but are also different from the 2D results of both (Sun et al., 2004; Sun et al., submitted for publication) where the lid heat flux was found to be independent of Peclet number. The differences may be ascribed to the fact that in the hydro-

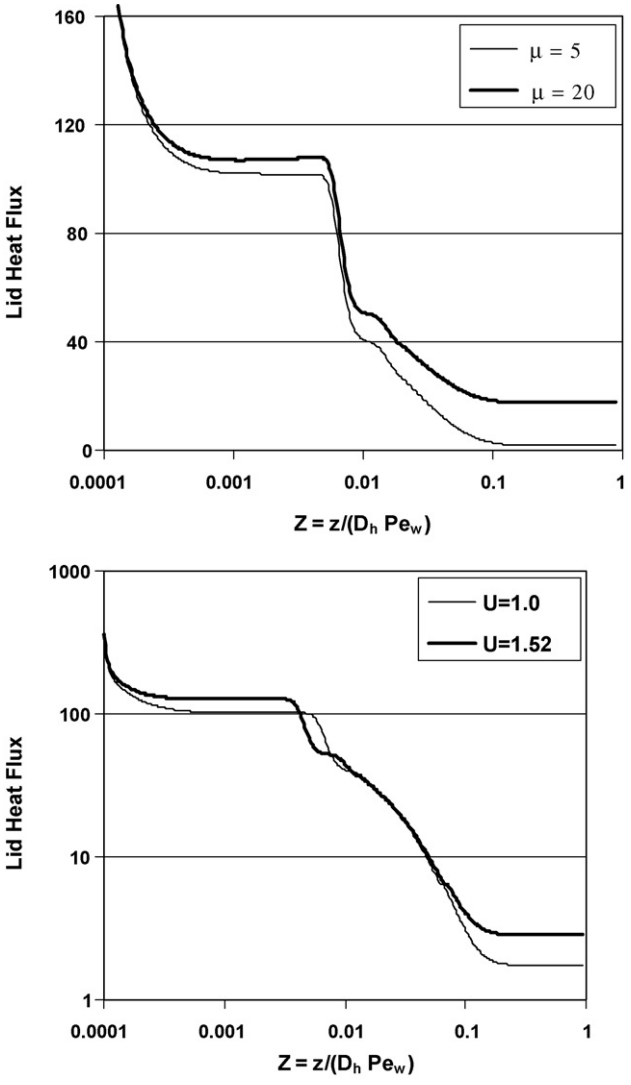

Fig. 8. Lid heat flux *Nu* for cooling of power law fluids with $n = 0.33$, $A = 0.2$ and $Br = 0.4167$: (top) effect of viscosity ($\mu = \mu_F$) and (bottom) effect of lid speed U.

dynamic and thermally developed 2D cases (Sun et al., 2004; Sun et al., submitted for publication) axial flow is neglected, and the tangential convection contributes only to the internal circulation, making no net contribution to the total heat transfer. In the quasi-3D case, where the axial and tangential flows interact, heat convected upstream also contributes to the total heat transfer.

Fig. 6b shows that the lid heat flux increases as the channel aspect ratio $A = H/L$ decreases. The plateau regions present in each of the curves once again indicate regions where the heat transfer is dominated by convection. The lid heat flux begins to decrease at a smaller value of Z for channels with larger values of A. For "thin" channels where A is small, an equilibrium temperature is reached more quickly; this is consistent with the results of Fig. 6b where, for a fixed value of Z, *Nu* is larger for channels with more extreme aspect ratios (i.e. smaller values of A).

Finally, the effect of characteristic viscosity μ_F (i.e. change in consistency index) and lid speed U on lid heat flux *Nu* are shown in Fig. 8. The lid heat flux is found to increase both with increasing characteristic viscosity and increasing lid speed. The now familiar plateau regions for small Z are also clearly present.

4. Conclusions

Finite element methods have been successfully used to study heat transfer for power law materials in lid driven channels with fully developed axial flow. Where comparison is possible, very good agreement is found between the numerical results and previously published data. Close to the singularity corners the velocity gradients are very large. For constant viscosity Newtonian fluids the viscous dissipation is therefore also very large. However, for shear thinning fluids the viscosity is reduced in high shear regions and the combined effects of high shear and low viscosity result in smaller viscous dissipation in shear thinning fluids than in Newtonian fluids. The fully developed wall heat flux and fluid temperature are therefore larger for Newtonian fluids than for shear thinning fluids. A practical consequence of this fact is that, for a given channel length the temperature at outlet is higher for Newtonian fluids than for shear thinning fluids.

Our results further show that the lid heat flux is dependent on the Peclet number. It increases as the viscosity increases, the lid velocity increases, and the channel aspect ratio decreases. When the Peclet number is large, extra mixing is required to remove heat trapped inside the circulation zones. Therefore to maintain a high lid heat flux a short heating section length is recommended. Another general trend to emerge from the results presented here is that, if accurate predictions of heat transfer are required, the coupling between the tangential and axial flows must be accounted for. 2D calculations cannot provide this and are therefore clearly insufficiently sophisticated if accurate quantitative results are required.

Finally, we note that in a real SSHE fluid leakage through the sidewalls may be present (for example, from adjoining chambers). If the associated effects of such flows are important, then it appears that there is little alternative to undertaking a full 3D analysis.

Acknowledgements

This research is supported by The University of Reading and Chemtech International, Reading. The authors are grateful for helpful insights provided by Dr. N. Hall-Taylor of Chemtech International and Professor M. Baines of Reading University.

References

Burggraf, O. R. (1966). Analytical and numerical studies of the structure of steady separated flows. *Journal of Fluid Mechanics*, *24*, 113–151.

Chandrupatla, A. R., & Sastri, V. M. K. (1997). Laminar forced convective heat transfer of a non-Newtonian fluid in a square duct. *International Journal of Heat and Mass Transfer*, *20*, 1315–1324.

Fastflo Tutorial Guide V3. (2000). Oxford, Numerical Algorithms Group.

Fitt, A. D., & Please, C. P. (2001). Asymptotic analysis of the flow of shear-thinning food stuffs in annular scraped heat exchangers. *Journal of Engineering Mathematics*, *39*, 345–366.

Grillet, A. M., Yang, B., Khomani, B., & Shaqfeh, E. S. G. (1999). Modelling of viscoelastic lid driven cavity flow using finite element simulations. *Journal of Non-Newtonian Fluid Mechanics*, *88*, 99–131.

Harrod, M. (1986). Scraped surface heat exchangers—A literature survey of flow patterns, mixing effects, residence time distribution, heat transfer and power requirements. *J. Food. Process. Eng.*, *9*, 1–62.

Hartnett, J. P., & Kostic, M. (1989). Heat transfer to Newtonian and non-Newtonian fluids in rectangular ducts. *Advances in Heat Transfer*, *19*, 247–356.

Karwe, M. V., & Jaluria, Y. (1990). Numerical simulation of fluid flow and heat transfer in a single screw extruder for non-Newtonian fluids. *Numerical Heat Transfer A*, *17*, 167–190.

Kokini, J. L., Ho, C.-T., & Karwe, M. V. (Eds.). (1992). *Food extrusion science and technology*. New York: Marcel Dekker, Inc.

Martin, B. (1969). *Numerical studies of steady state extrusion process*. Ph.D. thesis. Cambridge University.

Mitsoulis, E., & Zisis, T. (2001). Flow of Bingham plastics in a lid driven cavity. *Journal of Non-Newtonian Fluid Mechanics*, *101*, 173–180.

Nallasamy, M., & Prasad, K. K. (1977). On cavity flow at high Reynolds numbers. *Journal of Fluid Mechanics*, *79*, 391–414.

Pan, F., & Acrivos, A. (1967). Steady flows in rectangular cavities. *Journal of Fluid Mechanics*, *28*, 643–655.

Shankar, P. N., & Deshpande, M. D. (2000). Fluid mechanics in the driven cavity. *Annual Review of Fluid Mechanics*, *32*, 93–136.

Sun, K.-H., Pyle, D. L., Fitt, A. D., Please, C. P., Baines, M., & Hall-Taylor, N. (2004). Numerical study of 2D heat transfer in a scraped surface heat exchanger. *International Journal of Computers and Fluids*, *33*, 869–880.

Sun, K.-H., Pyle, D. L., Fitt, A. D., Please, C. P., Hall-Taylor, N., & Baines, M. (submitted for publication). Numerical modelling of non-Newtonian heat transfer with viscous dissipation in lid driven cavities. *AIChE Journal*.

Sun, K.-H., Pyle, D. L., Hall-Taylor, N., Baines, M. J., & Fitt, A. D. (2006). Velocity profiles and frictional pressure drop for shear thinning materials in lid driven cavities with fully developed axial flow. *Chemical Engineering Science*, *61*, 4697–4706.